Investigation of a gas-fuelled water heater based on combined power and heat pump cycles

Youcai Liang, Mohammed Al-Tameemi, Zhibin Yu*

Systems, Power & Energy Research Division, School of Engineering, University of Glasgow, Glasgow G12 8QQ, UK

* Corresponding author: Tel.: +44 (0) 141 330 2530; E-mail address: Zhibin.Yu@glasgow.ac.uk

Abstract

In this paper, we proposed and demonstrated a novel gas-fuelled hot water system based on combined power and heat pump cycles. It essentially integrates a premixed gas burner, an organic Rankine cycle (ORC) power plant, and an air source heat pump for supplying hot water. An ORC power plant generates mechanical power from the thermal energy produced from the combustion of natural gas in the burner. Subsequently, the generated power directly drives a vapour compression cycle heat pump through a common shaft connecting the expander and the compressor. Cold tap water is headed firstly in the condenser of the heat pump, then in the condenser of the ORC power plant, and finally the flue gas exiting from the burner in a post heater. The flue gas exiting the post heater will be mixed with ambient air to further extract its residual heat in the evaporator of the heat pump. The advantages of the proposed system are threefold. First, the waste heat of the power cycle has been fully recovered. Second, the heat pump operates on a much lower temperature difference, leading to

higher *COP*. Third, it has no electrical generator or motor, avoiding the transduction losses. A comprehensive analysis has been presented in this paper, and the results show that the proposed system can achieve an overall fuel-to-heat efficiency up to 147% when the cold water is heated from 10 to 65 °C and the ambient air temperature is in the range -5 to 5 °C. The research results demonstrated that the proposed technology has a great potential for hot water applications.

Keywords: Organic Rankine cycle; air source heat pump; water heater; combined cycles

1. Introduction

In order to mitigate the risks of climate change resulting from global warming, it is important to reduce the energy consumption and greenhouse gas emissions. Heating accounts for a large part of the energy consumption in countries with cold winters (e.g., UK), and it usually heavily relies on the burning of fossil fuels such as natural gases and coal. The decarbonisation of the heating sector is therefore pivotal, but it is far more challenging than the power sector due to its nature of decentralised generation and consumption.

There is a wide range of technologies at different stages of development for heating applications, including electrical resistive heaters, gas boilers, heat pumps (HPs), and micro-CHP (combined heat and power) systems. They all have different fuel-to-heat efficiencies that are defined as the ratio of the useful heat production to the energy contained in the consumed fossil fuels [1, 2].

Nowadays, most installed gas boilers are condensing boilers, which have a fuel-to-heat efficiency of around 90% by recovering some heat from their flue gases [2]. Electrical resistive heaters have near 100% efficiency to convert electricity to heat, but their fuel-to-heat efficiency maybe only around 32-40% if electricity is generated from fossil fuels [3]. An electrically driven heat pump (HP) is an ideal alternative technology for domestic heating if low carbon electricity is supplied. However, to achieve any saving of carbon emissions relative to gas boilers, the HP would require a Coefficient of Performance (*COP*) of over 2.5 with the current electricity supply mix in the UK [4]. In fact, the air source and ground source HPs installed in the UK to

55 date have *COP* in the range of 1.2 to 3.3 [5]. Fossil-fuelled power plants have an
56 efficiency in the range of 34-42%, and the loss in electricity transmission and
57 distribution is about 6% [6]. Assuming an average *COP* of 2.5, the overall fuel-to-heat
58 efficiency of an electrically powered HP would be only around 80-100%.

59 Gas-driven absorption HPs have been successfully used in large-scale district
60 heating applications [4]. Domestic scale gas-driven absorption HPs have recently
61 been introduced to the European market, claiming a fuel-to-heat efficiency around
62 130-150% [7]. Gas-driven adsorption HPs have also been researched recently, and
63 they were reported to have a fuel-to-heat efficiency about 130% in laboratory [7]. Air,
64 water or waste water, soil, geothermal borehole can all be used as heat sources for
65 heat pumps for different applications. Great efforts had been made to improve the
66 performance of heat pumps in the past several decades.

67 For air source heat pump, the operation parameters and control strategy influence
68 the system performance significantly. Fischer et al. [8] studied the effect of different
69 control strategies and boundary conditions on the performance of heat pumps and
70 recommended the trade-off between system complexity and performance. A
71 self-optimizing control scheme was proposed by Hu et al. to improve the system
72 performance of an air-source heat pump by using the extremum seeding control
73 strategy, which is adopted to match the varying ambient temperatures, water outlet
74 temperatures and discharge pressure [9]. Gupta and Irving [10] developed a model
75 that can respond to the changing temperatures of the heat source and sink and their
76 study showed correct response to the changing ambient temperature.

77 Despite the continuous progresses made in improving the heat pump's
78 performance, there are still challenges in the practical applications of heat pumps. One
79 is to overcome the low *COP* issue due to the high-temperature lift in winter to reach a
80 desired temperature over 65°C [11]. The poor performance of heat pumps due to high
81 condensation temperature has become a significant obstacle. Furthermore, wide
82 installation of electrically-powered heat pumps will increase peak electricity demand
83 in winter [12, 13], bring challenges to the electrical grid.

84 The idea of combining power generation cycles and heat pump cycles has been
85 investigated in the past. A concept of ORC driven heat pump system using the same
86 working fluid and sharing a condenser was proposed by Strong [14]. Later on,
87 experimental investigation of this concept was carried out by Demierre et al. [15, 16].
88 Recently, a hybrid gas engine-driven heat pump system was proposed by Wan et al.
89 [17] and its primary energy ratio, the ratio of the useful energy output to the primary
90 energy input, can achieve up to 1.09. Shang et al. [18] analysed another type of hybrid
91 power-driven heat pump system theoretically. The results showed that the primary
92 energy ratio is 15.8-25.3% higher than that of the conventional gas engine-driven heat
93 pump system by introducing waste heat recovery.

94 Combined heat and power (CHP) systems for meeting electric and heat demands
95 in cold climate regions have also been widely investigated. Cho et al. [19] performed
96 a conceptual study of a heat pump driven by a CHP system for producing hot water in
97 parallel. It however has a relatively low theoretical *COP* of 3.6-4 because the heat
98 pump operates at large temperature lift. Kang et al. [20] also analysed a parallel

system that uses a gas turbine to drive a heat pump and recovers the gas turbine's waste heat to produce hot water, but this system again suffers from a lower heat pump COP due to a high condenser temperature. Schimpf and Span [21] numerically analysed a heat pump system that is capable of running in reverse as an ORC by diverting the working fluid between an expansion valve and pump, depending on the flow direction. However, their ORC system does not directly power the heat pump, and the waste heat of the ORC system is used to recharge a geothermal heat source. Liu et al. [22] analysed a system that uses an internal combustion engine to directly drive a heat pump, but the waste heat of the IC engine was used to drive an ORC to generate power instead of heating water. In addition, Siviter [23] proposed to use thermoelectric heat pumps in the condensation process of the Rankine cycle to improve the system performance, and the experimental results showed the potential this concept.

In this paper, we propose a novel natural gas fuelled hot water heater based on combined power and heat pump cycles. The proposed system essentially integrates a premixed gas burner, an ORC power plant, and an air source heat pump for supplying hot water. The thermal energy produced from natural gas in the burner powers an ORC power plant. Subsequently, the generated power directly drives a vapour compression heat pump. Cold tap water is heated by three heat exchangers in series to gradually increase its temperature. It is preheated in the condenser of the heat pump, then heated in the condenser of the ORC power plant, and finally further heated by the flue gas exiting from the burner in a post heater. The flue gas exiting the post heater

will be mixed with fresh ambient air to further extract its residual heat. In response to the changing ambient air temperatures, the proposed system can adjust the mass flow rates of the natural gas to the burner and the fresh air to mix with the flue gas to ensure hot water supply at a temperature of 65 °C.

The proposed water heater has several advantages. First, the waste heat of the power cycle has been fully recovered. Second, such an ORC-HP system design enables the heat pump to work at a much lower condensing temperature than that of a conventional heat pump for supplying hot water at the same temperature, leading to a higher *COP*. Third, the mechanical power of expander of the ORC cycle directly drives the compressor of the heat pump, so it eliminates the electrical generator or motor, and thus avoids the transduction losses. Fourth, it can maximise the heat recovery from the flue gases, further improving the system's efficiency.

2. Concept

As shown in Fig. 1, the proposed system integrates an ORC power plant and a vapour compression heat pump. The thermal energy released by the combustion of natural gas is transferred to power the ORC system through the Evaporator-ORC. Cold tap water is preheated in the Condenser-HP, and is then further heated in Condenser-ORC. Finally, it reaches the required supply temperature in the post heater that further recovers heat from the flue gases. After leaving the post heater, the flue gases then mixes with fresh air, entering the Evaporator-HP where their residual heat will be further extracted.

Unlike the conventional CHP systems that drive a generator to produce electricity, the power generated by the ORC is used to directly drive the compressor of a heat pump. The compressor of heat pump and the expander of ORC are directly connected with a common shaft.

The main interests in this paper is to investigate the theoretical limit of performance of the proposed system using available working fluids. A screen of working fluids showed that the best performance was achieved in the simulations when hexane and R134a were used as the working fluid for the ORC system and heat pump, respectively. In fact, some researchers have studied the potential of hexane for ORC power plants [24-26], but it has not been widely used in practical applications so far due to its flammability. On the one hand, as the technologies advance, solutions can be developed to address this challenge. For example, mixing hexane with retardant working fluid can potentially maintain its high efficiency while overcome the concerns of its flammability. On the other hand, flammable working fluids such as propane have already been used for high temperature heat pumps [27-29]. Hence, the results based on the pair of hexane and R134a have been used in this paper to demonstrate the best performance we can achieve in theory using the proposed system.

The Temperature-Entropy diagrams of two thermodynamic cycles are shown in Fig. 2. The green line refers to water, pink for R134a, blue for hexane, red for the flue gas, and nattier blue for the mixture of fresh air and flue gas. Hexane is a dry working fluid and thus only minimal superheat is needed [30, 31].

3. Theoretical Model

A programme based on Matlab platform and Refprop database is developed to analyse the thermodynamic performance of the system as shown in Fig. 1. The enthalpies and entropies at different states were calculated by using a database Refprop 9.0. An Aspen Plus model was also used to verify the present Refprop/Matlab model.

The main assumptions used in the modelling are listed as follows.

(1) The combustion efficiency is assumed to be 100%.

(2) Nitrogen does not take part in the chemical reaction during the combustion process.

(3) Both heat and pressure loss in all heat exchangers and pipes are negligible.

(4) The combined cycles are operated under steady state conditions.

(5) The temperature of flue gas is higher than the acid dew point at the outlet of post heater

(6) The Evaporator-HP is made of anticorrosion materials.

(7) There is no power loss at the common shaft between the expander and the compressor.

(8) The natural gas is assumed to be pure methane.

(9) Assume sufficient excessive air will be supplied to ensure the temperature of combustion products in the evaporator will low enough to prevent the decomposition of the working fluid.

The design target is to provide domestic hot water at 65°C. The proposed system is scalable, and is preferred for relatively large applications. For the convenience of experimental research in the laboratory, the heating power is set as 20 kW in this research. Some other main operating parameters are listed in Table 1.

3.1 Gas burner

The fuel considered in this study is natural gas and it is assumed to be pure methane. The complete reaction combustion of natural gas can be expressed as:

$$CH_4 + 2(1+\alpha)(O_2 + 3.76N_2) \rightarrow CO_2 + 2H_2O + 7.52(1+\alpha)N_2 + 2\alpha O_2 \quad (1)$$

$$\lambda = 1 + \alpha \quad (2)$$

Here, α refers to the amount of excess air and λ refers to the excess air ratio [32]. The excess air ratio for natural gas combustion is normally in the ranges of 1.05-1.2 [32-35]. The excess air ratio is set as 1.2 in this study.

For a constant-pressure equilibrium process, the heat released during the combustion process can be defined as:

$$Q_{comb} = \Delta H \cdot m_{fuel} \quad (3)$$

$$\Delta H = H_P - H_R \quad (4)$$

Here, H_P is the enthalpy of the products of combustion that leave the combustion chamber and H_R is the total enthalpy of the reactants that enter it. The combustion heat of methane is 890.3 kJ/mol. The model of the combustion process of natural gas is validated using the data presented in reference [36]. The predicted combustion temperature for this model is 2332 K when the excess air ratio is 1, slightly different

from 2328 K as predicted in Ref [36]. According to the reaction process as shown in Equation (1), when the excess air ratio is 1.2, the mass fractions of CO_2, H_2O, N_2 and O_2 are 6.35%, 5.20%, 75.22% and 13.23% in the product mixture, respectively.

After the combustion process in the burner, additional air will be added to the combustion products to reduce their temperature to the required temperature range 260-280 °C [37] to avoid the decomposition of the refrigerant in Evaporator-ORC.

3.2 Pinch-point temperature difference method

The limitation of pinch point temperature difference was considered in the modelling of all heat exchangers during phase change processes to ensure the feasible heat exchanger design in practical applications. Take the evaporation process in the Evaporator-ORC for example, the temperature of flue gas at evaporator inlet (T_5), the temperature of hexane at the evaporator inlet (T_2), the mass flow rate of flue gas (m_g) and the minimum pinch point temperature difference (ΔT_{pp}) are all pre-set. Assuming the bubble point is the pinch point so T_A=T_B+ΔT_{pp}, and the mass flow rate of hexane can be calculated based on the energy conservation as:

$$m_f = \frac{c_{pg} \cdot m_g \cdot (T_5 - T_A)}{h_3 - h_B} \tag{5}$$

Then the energy balance during the process from state 2 to state B can determine the temperature T_6 as:

$$T_6 = T_A - \frac{m_f \cdot (T_B - T_1)}{c_{pg} \cdot m_g} \tag{6}$$

,

where the c_{pg} refers to the specific heat capacity of flue gas.

A procedure was developed to compare the (T_6-T_2) and (T_A-T_B). If (T_6-T_2)>(T_A-T_B), it means that the assumption of pinch point locating at the bubble point is reasonable. Otherwise, the Pinch Point locates at state 6 and T_6=T_2+ΔT_{pp}. If (T_6-T_2)<0, T_6 calculated with Equation (6) is lower than the acid dew point of the flue gas, then there is no pinch point limitation in the heat exchange process which limits the amount of heat transfer to the ORC needed to avoid overcooling of the flue gas [38], to ensure T_6 is higher than 120 °C to avoid the acid dew point in the boiler. This pinch point temperature difference (PPTD) method is also adopted in all the other heat exchangers.

3.3 Organic Rankine cycle

The modelling of four main components in the basic ORC is present as follows. The working fluid is pumped from low to high pressure by the pump that consumes mechanical work, and it can be calculated as:

$$W_{p-ORC} = m_f \cdot (h_2 - h_1) / \eta_p \quad (7)$$

Wherein, η_P refers to the isentropic efficiency of the pump.

The high-pressure liquid enters Evaporator-ORC where it is heated to a saturated vapour at constant pressure. The heat transfer within the Evaporator-ORC can be calculated as:

$$Q_{eva-ORC} = m_f \cdot (h_3 - h_2) \quad (8)$$

$$Q_{eva-ORC} = m_e \cdot (h_5 - h_6) \quad (9)$$

High temperature and pressure vapour of the working fluid expands during the process 3-4 and the generated power can be calculated as:

$$W_{ORC} = m_f \cdot (h_3 - h_4) \cdot \eta_T \quad (10)$$

Wherein, η_T refers to the isentropic efficiency of the turbine.

The vapour enters the Condenser-ORC where it condenses at a constant pressure to turns into a saturated liquid. The heat transfer to water within the Condenser-ORC can be expressed as:

$$Q_{con-ORC} = m_f \cdot (h_4 - h_1) \quad (11)$$

$$Q_{con-ORC} = m_w \cdot (h_{13} - h_{12}) \quad (12)$$

Wherein, m_w refers to the mass flow rate of water.

In our initial design, the post heater aims to further increase the temperature of the hot water and the heat transfer can be expressed as:

$$Q_{post} = m_w \cdot (h_{16} - h_{13}) \quad (13)$$

3.4 Vapour compression cycle heat pump

The two-phase refrigerant turns into vapour by absorbing heat from the mixture of fresh air and flue gas in Evaporator-HP, the heat transfer within the Evaporator-HP can be calculated as:

$$Q_{eva-HP} = m_r \cdot (h_7 - h_{10}) \quad (14)$$

$$Q_{eva-HP} = c_{pm} \cdot m_{mix} \cdot (T_{14} - T_{15}) \quad (15)$$

Wherein, m_r and m_{mix} refer to the mass flow rate of refrigerant and the mixture gas respectively, c_{pm} refers to the specific heat capacity of gas mixture.

The vapour of refrigerant R134a is then pressurised and circulated by a compressor. The power required is provided by the ORC expander. It can be calculated as:

$$W_{com} = m_r \cdot (h_8 - h_7) \quad (16)$$

$$W_{com} = W_{ORC} \quad (17)$$

W_{com} and W_{ORC} refer to the mechanical work consumed by compressor and the mechanical work generated in ORC, respectively.

The high-pressure R134a vapour rejects its heat to the water and turns into liquid. The heat transfer can be calculated as:

$$Q_{con-HP} = m_r \cdot (h_8 - h_9) \quad (18)$$

$$Q_{con-HP} = m_w \cdot (h_{12} - h_{11}) \quad (19)$$

The liquid refrigerant R134a exiting the Condenser-HP expands then changes into a low-pressure, low-temperature, two-phase mixture. It can be assumed as an isenthalpic process as the following.

$$h_9 = h_{10} \quad (20)$$

3.5 Evaluation of the system

Thermal efficiency of the ORC is defined as:

$$\eta_{ORC} = \frac{W_{ORC} - W_{p-ORC}}{Q_{eva-ORC}} \quad (21)$$

The Coefficient of Performance (*COP*) of heat pump is defined as:

$$COP = \frac{Q_{con-HP}}{W_{com}} \quad (22)$$

The total heat output of hot water heater can be calculated as:

$$Q_{total} = m_w \cdot (h_{16} - h_{11}) \quad (23)$$

The overall fuel-to-heat efficiency can be defined as:

$$\eta_{f-h} = \frac{Q_{total}}{Q_{comb}} \quad (24)$$

3.6 Heat transfer area of the heat exchangers

According to the calculated heat capacity, the heat transfer area of the heat exchangers can then be determined [39]. Plate heat exchangers are chosen for the Condenser-ORC, condenser-heat pump, and the post heater owing to its efficient heat transfer and compactness. Hence, all the simulations below are based on plate heat exchangers.

3.6.1 Correlation for working fluid in single-phase state

For the fluid in the sub-cooling zone (state 2 to state B) and in the sup-heating zone (state 8 to state E, and state 4 to state C), heat transfer coefficient (α_f) can be calculated according to a semi-empirical equation that is based on Leveque analogy and experimental data [40] as follows.

$$\mathrm{Re} = \rho \cdot \upsilon \cdot d_{eq} / \mu \tag{25}$$

$$\mathrm{Pr} = c_p \cdot \mu / k \tag{26}$$

$$1/ f^{0.5} = \cos\beta / (0.18 \cdot \tan\beta + 0.36 \cdot \sin\beta + f_0 / \cos\beta)^{0.5} + (1 - \cos\beta) / (3.8 \cdot f_1)^{0.5} \tag{27}$$

When $\mathrm{Re} < 2000$, $f_0 = 64/\mathrm{Re}$, $f_1 = 579/\mathrm{Re} + 3.85$

When $\mathrm{Re} \geq 2000$, $f_0 = (1.8 \cdot \lg \mathrm{Re} - 1.5)^{-2}$, $f_1 = 39/\mathrm{Re}^{0.289}$

$$Nu = 0.122 \cdot \mathrm{Pr}^{1/3} \cdot (\mu / \mu_{wall})^{1/6} (f \cdot \mathrm{Re}^2 \cdot \sin 2\beta)^{0.374} \tag{28}$$

$$\alpha = Nu \cdot k / d_{eq} \tag{29}$$

$$d_{eq} = 2b_1 / \varphi \tag{30}$$

Here, Re, *Nu* and Pr refer to the Renold number, Nusselt number and Prandtl number respectively; d_{eq} refers to the equivalent diameter of working fluid channel; b_1 is corrugation depth and φ is the surface enlargement factor of a plate heat exchanger. Table 2 summarises the main geometric dimensions of the plate heat exchangers.

The correlation mentioned above can be also adopted to calculate the heat transfer coefficient (α_w) of the cold-water side. Cooper's pool boiling correlation is adopted for the heat transfer coefficient (α_g) calculation of the evaporating phase change process [40]:

$$\alpha_e = 1.5 * 55 \cdot (p_e / p_{cr})^{(0.12 - 0.2 \cdot \lg Rp)} \cdot (-\lg(p_e / p_{cr}))^{-0.55} \cdot q^{0.67} \cdot M^{-0.5} \tag{31}$$

Here, p_e and p_{cr} mean evaporating pressure and the critical pressure of working fluid (MPa), respectively; *Rp* means the mean asperity height (μm). According to the supplied plate heat exchanger, the value of *Rp* is 0.3 in this calculation; *q* means the heat flux (W/m^2), M means the molar mass of working fluid (kg/kmol).

3.6.2 Correlation for condensation process

The condensation heat transfer coefficient (α_c) of all working fluids can be calculated by using the following correlation [41]:

$$\alpha_l = 0.2092 \cdot (k_l / d_{eq}) \cdot \mathrm{Re}_l^{0.78} \cdot \mathrm{Pr}_l^{0.33} \cdot (\mu / \mu_{wall})^{0.14} \quad (32)$$

$$\mathrm{Re}_l = G \cdot d_{eq} / \mu_l \quad (33)$$

$$\mathrm{Pr}_l = cp_l \cdot \mu_l / k_l \quad (34)$$

$$Co = (\rho_v / \rho_l) \cdot (1/x - 1)^{0.8} \quad (35)$$

$$Fr_l = G^2 / (\rho_l^2 \cdot g \cdot d_e) \quad (36)$$

$$Bo = q / G \cdot i_{fg} \quad (37)$$

$$\alpha = \alpha_l \cdot (0.25 \cdot Co^{-0.45} Fr_l^{0.25} + 75 \cdot Bo^{0.75}) \quad (38)$$

Here,

C_0 – Convection number;

B_0 – Boiling number;

x – Quality;

G– Mass flux of the working fluid (kg/m^{2}s);

g– Acceleration due to gravity (m/s^2);

i_{fg}– Enthalpy of vaporization (kJ/kg).

Based on the heat transfer coefficient above, the heat transfer area can be obtained as:

$$A = Q / K / \Delta T_m \quad (39)$$

$$1/K = 1000/\alpha_{hot-side} + t/\lambda + 1000/\alpha_{cold-side} \quad (40)$$

When $\Delta T_1 > \Delta T_2$, then

$$\Delta T_m = \frac{\Delta T_1 - \Delta T_2}{\ln(\Delta T_1 / \Delta T_2)} \quad (41)$$

Wherein,

$$\Delta T_1 = T_{1in} - T_{2out} \quad (42)$$

$$\Delta T_2 = T_{1out} - T_{2in} \quad (43)$$

Here, subscript 1 means the hot fluid, 2 means the cold fluid, subscript "in" means at the inlet, "out" means the outlet.

3.6.3 Correlation for Evaporator-HP and post heater

As is well known, the heat transfer coefficient on the gas side is much lower than those on the liquid side. A fin and tube heat exchanger is adopted to increase heat transfer area by utilizing finned heat transfer surfaces. The modelling of the Evaporator-HP is set up based on the fin and tube heat exchanger. The main geometric dimensions of fin and tube heat exchange is shown in Table 3.

For the fin side (namely the air side), the heat transfer fluid is a mixture of fresh air and flue gases. In order to further recover heat from the flue gases, all the exhaust gases pass through the Evaporator-HP. Fresh air is mixed with flue gases to provide sufficient heat energy needed in the evaporator. The flow rate of fresh air is determined by the required heat in Evaporator-HP and temperature difference between inlet and outlet.

The equivalent heat transfer coefficient of the fin side is expressed as:

$$\alpha_{of} = \xi \cdot \alpha_o \cdot \eta_s \quad (44)$$

ξ – The moisture absorption coefficient;

376 α_o – Heat transfer coefficient of air side;

377 η_s – Surface effectiveness;

378 The moisture absorption coefficient ξ is expressed as follows. If $d_{am} > d_{we}$,

379 $\xi = 1 + \frac{2460 \cdot (d_{am} - d_{we})}{t_{am} - t_{we}}$, Where, $t_{am} = \frac{t_{a1} - t_{a2}}{2}$, t_{a1}, t_{a2} are the mixture temperatures

380 at inlet and outlet. If $d_{am} < d_{we}$, $\xi = 1$. d_{am} and d_{we} refer to the mean humidity ratio of

381 the moist air and humidity ratio of saturated air respectively, and t_{am} and t_{we} are the

382 mean temperature of the moist air and the wall temperature of tube respectively.

383 The surface effectiveness η_s can be calculated as:

384 $$\eta_s = 1 - \frac{a_f}{a_a}(1 - \eta_f) \tag{45}$$

385 a_f – the area of the fin per meter of the tube, $a_f = \frac{2(S_1 \cdot S_2 - \pi \cdot d_b^{\,2})}{S_f}$;

386 a_b – The external surface area of tube per meter tube, $a_b = \frac{\pi \cdot d_b \cdot (S_f - \delta_f)}{S_f}$;

387 d_b – The external diameter of fin collar, $d_b = d_0 + 2\delta_f$;

388 a_a – The total area of the heat exchanger per unit, $a_a = a_f + a_b$;

389 S_1 – Depth of the heat exchanger perpendicular to airflow direction;

390 S_2 – Depth of the heat exchanger in airflow direction, $S_2 = \frac{\sqrt{3} S_1}{2}$;

391 d_0 – External diameter of tube;

392 δ_f – Thickness of the fin;

393 S_f – Fin spacing;

394 The fin effectiveness η_f is defined as:

$$\eta_f = \frac{\tanh(m \cdot h')}{m \cdot h'} \tag{46}$$

where $m = \sqrt{\frac{2 \cdot \xi \cdot \alpha_o}{\lambda_{al} \cdot \delta_f}}$.

The equivalent height of the fin $h' : h' = 0.5 d_b \cdot (\rho' - 1) \cdot (1 + 0.35 \ln \rho')$

For the staggered finned tube banks ρ', $\rho' = 1.27 \frac{s_1}{d_b} \sqrt{\frac{l_1}{l_2} - 0.3}$

l_1 – The long side of the hexagon fin;

l_2 – The short side of the hexagon fin;

In this case, $l_1 = l_2$ for the Equilateral hexagon.

The heat transfer coefficient of air side can be expressed as:

$$\alpha_o' = C \cdot \frac{\lambda_f}{d_{eq}} \cdot \mathrm{Re}_f^n \cdot \left(\frac{S_2}{d_{eq}} \right)^m \tag{47}$$

Here,

$$\mathrm{A} = 0.518 - 0.02315(\frac{S_2}{d_{eq}}) + 0.000425(\frac{S_2}{d_{eq}})^2 - 3*10^{-6}(\frac{S_2}{d_{eq}})^3;$$

$$C = A \cdot (1.36 - \frac{0.24 \mathrm{Re}_f}{1000});$$

$$n = 0.45 + 0.0066 \frac{S_2}{d_{eq}};$$

$$m = -0.28 + 0.08 \frac{\mathrm{Re}_f}{1000};$$

Wherein,

$$d_{eq} = \frac{2(S_1 - d_o) \cdot (S_f - \delta_f)}{(S_1 - d_o) + (S_f - \delta_f)};$$

$$\mathrm{Re}_f = \frac{w_{\max} \cdot d_{eq}}{\upsilon_f};$$

Wherein,

υ_f –Kinematic viscosity, m^2/s;

w_{max} – The wind velocity flowing through the narrowest area,

$$w_{\max} = \frac{S_f \cdot S_1 \cdot w_f}{(S_1 - d_b) \cdot (S_f - \delta_f)};$$

Therefore, the equivalent heat transfer coefficient of fin side can be expressed as:

$$\alpha_o = \alpha_o' \cdot k_1 \cdot k_2 \quad (48)$$

k_1 – Correction coefficient of configuration, k_1=1.1 for staggered arrangement;

k_2 – Correction coefficient of fin style, k_2 =1.2 for wavy fin;

(1) The heat transfer coefficient of tube side

The tube side heat transfer coefficient α_i for Evaporator-HP is evaluated from Kandlikar correlation [41, 42].

$$\frac{\alpha_i}{\alpha_l} = C_1 \cdot (C_0)^{C_2} \cdot (25F \cdot r_l)^{C_5} + C_3 \cdot (B_0)^{C_4} \cdot F_{fl} \quad (49)$$

Wherein,

α_l – The heat transfer coefficient of the liquid refrigerant flowing in the tube,

$$\alpha_l = 0.023\left(\frac{g \cdot (1-x) \cdot d_t}{\mu_l}\right)^{0.8} \frac{\mathrm{Pr}_l^{0.4} \cdot \lambda_l}{d_l};$$

C_0 – Convection number, $C_0 = \left(\frac{1-x}{x}\right)^{0.8} \cdot \left(\frac{\rho_g}{\rho_l}\right)^{0.5}$;

B_0 – Boiling number, $B_0 = \frac{q}{g \cdot r}$;

F_{rl} – Froude number with all flow as liquid, $Fr_l = \frac{g^2}{9.8\rho_l^2 \cdot d_l}$;

g – Mass flow per unit area per unit time, $kg/(m^2 \cdot s)$;

λ_l – Thermal conductivity of liquid phase, $W/(m \cdot K)$;

P_{rl} – Prandtl number of liquid phase;

ρ_g – Density of gas phase, kg/m^3;

x – Quality;

q – Heat flux, w/m^2;

ρ_l – Density of liquid phase, kg/m^3;

F_{fl} – Determined by working fluid, for R134a, F_{fl}=1.63;

if C_0<0.65, C_1=1.136, C_2=-0.9, C_3=667.2, C_5=0.3;

if C_0>0.65, C_1=0.6683, C_2=-0.2, C_3=1058.0, C_5=0.3;

The overall heat transfer coefficient can be determined from the knowledge of the inside (tube side) and outside (fin side) heat transfer coefficient.

$$K_{fin-tube} = \frac{1}{\frac{1}{\alpha_i}\cdot\frac{a_f}{a_i} + \frac{\delta_f}{\lambda}\cdot\frac{a_{of}}{a_m} + r_b + r_o + \frac{1}{\alpha_o\cdot\eta_s}} \tag{50}$$

λ – Thermal conductivity of brass, 383W/m·K;

r_0 – thermal resistance, 0.001 m^{2}K/W;

r_b – contact resistance of between the fin and the tube, 0.0048;

Based on the heat transfer coefficient above, the heat transfer area of fin side can be obtained as:

$$A_o = Q / K_{fin-tube} / \Delta T_m \tag{51}$$

$$A_i = A_o / (\frac{a_a}{\pi d_i}) \tag{52}$$

$$l = A_o / a_a \tag{53}$$

d_i – Internal diameter of tube;

452 A_i – Heat transfer area of tube;

453 d_i – Heat transfer area of fin;

454 l – Length of tube;

455 ΔT_m – Logarithmic mean temperature difference, LMTD.

456

457 **4. Results and discussions**

458 **4.1 Comparison between two models**

459 The proposed system was modelled using both ASPEN Plus and the present
460 Refprop/Matlab code, based on the same working condition. In order to compare the
461 simulations of the proposed system using these two models, we selected one case with
462 the evaporating temperature of the heat pump T_{eva2} = 270.33 K, the temperature of the
463 gas mixture exiting the Evaporator-HP T_{15}=275.55 K, and an ambient air temperature
464 of T_0=278.15 K. Tables 4 and 5 show the comparison between the key parameters
465 calculated using these two models.

466 Table 4 summarises the calculated the temperatures, heat transfer, work transfer
467 within the key components of the proposed system, as well as the difference between
468 the two models. An Aspen plus model is used as the benchmark. The calculated
469 temperature using these two models are all very close to each other, and the
470 differences are all less than 1%. It can also be seen that there is only very small
471 difference (namely <4.8%) in the calculated heat transfer at each heat changers
472 between the predictions by the two models. This can be attributed to the different
473 control strategies and the different PPTD approaches used for calculating the heat

474 transfer. For example, the heat absorbed by water in the Condenser-HP ($Q_{con2\text{-}HP}$)
475 predicted by Aspen plus model is 1.5 % higher than that of the present model, while
476 the heat rejected by the Condenser-ORC calculated by the Aspen plus model is 4.8%
477 lower than that of the present model. For the Aspen Plus model, the water temperature
478 T_{16} is controlled directly by adjusting the mass flow rate of the fuel, while for the
479 present Refprop/Matlab model, both the temperature of flue gas T_6 and the mass flow
480 rate of natural gas can be adjusted.

481 Table 5 shows the calculated performance indicators of this case study using
482 these two models. The *COP* of the heat pump subsystem calculated by the Aspen
483 model is around 5.7 % higher than that predicted by the present model, while the
484 thermal efficiencies predicted by two models are almost the same. The total heat
485 power output predicted by the present model is 1.4 % higher than the Aspen plus
486 model. The predicted overall fuel-to-heat energy efficiencies are almost the same.

487 Nevertheless, the results shown in Table 4 and 5 demonstrate a good agreement
488 between the results calculated using these two models, offering us the confidence to
489 use the present model to further analyse the performance and characteristics of the
490 proposed system. In this study, Refprop/Matlab is adopted in the following analysis
491 since the modelling of each component and the control strategy sometimes are not
492 available for the Aspen Plus model, which is a disadvantage for the designing and
493 system optimization. However, the Refprop/Matlab model can overcome this
494 disadvantage. This is the reason why Refprop/Matlab model was adopted.

495

4.2 Comparison of system performance using different ORC working fluids

The performance of thermodynamic cycles strongly depend on the properties of working fluids. Ideally, the working fluids should meet a list of criteria such as stability, non-fouling, non-corrosiveness, non-toxicity and non-flammability. However, not all the desired criteria could be satisfied in the present ORC design. Dreschler et al. [43] proposed working fluid selection based on thermal efficiency as the key criterion.

A comparison of system performance between R245fa, R123 and hexane are conducted and the result are shown in Table 6. The system with different working fluids are assumed to operate under the same working conditions. The evaporation pressure and condensation temperature of ORC are set to be 3000 kPa and 61 °C, respectively.

There are three parameters to evaluate the system performance, thermal efficiency for ORC, COP for heat pump cycle, and the overall fuel-to-heat efficiency for the whole system. It can be seen in Table 6 that the maximum thermal efficiency of ORC can be obtained by using hexane and that the maximum COP can be obtained by using R245fa. The maximum fuel-to-heat efficiency was achieved using hexane when the ambient temperature is in the range from -5 °C to 5 °C. In order to explore theoretical limit of performance of this system, hexane is used as the ORC working fluid in the following. As explained early on, although the hexane is flammable, mixing hexane and retardant working fluid is a possible way to maintain its high efficiency but overcome the issues of its flammability.

4.3 Effects of the ambient air temperature and the condensation temperature of the ORC

Using the obtained model that has been verified by Aspen Plus to some extent, a set of comprehensive simulations has then conducted to optimise the proposed system in response to the changing ambient temperatures. The design target is to heat cold tap water from 10 to 65 °C and deliver 20 kW heating power when the ambient air temperature varies in the range from -5 to 5 °C. The condensation temperature of ORC T_{con1} is an important parameter that strongly affects the water temperature T_{13}, the exiting temperature of flue gas T_6, and then the final hot water temperature T_{14}. Therefore, the effects of the ambient temperature T_0 and the condensation temperature T_{con1} on the performance of the whole system are studied in detail. The evaporation pressure within the Evaporator-ORC is set at 3000 kPa since the ORC can obtain relatively high thermal efficiency when it is operated closed to the critical pressure.

In practical applications, mass flow rates of pumps or compressors are usually used to control the operation of thermodynamic systems. There are three fluids exchanging energy with the system, including natural gas, fresh air, and water. The mass flow rate of water is 0.087 kg/s and both the temperature of cold tap water and the target temperature are set as 10 and 65 °C, respectively. So only the mass flow rates of natural gas and fresh air are variable. In this system, the mass flow rate of natural gas is controlled to match the system with the changing ambient air temperature.

As shown in Fig. 3, the mass flow rate of natural gas decreases as ambient air temperature increases from -5 to 5 °C for any given condensation temperature within the Condenser-ORC. More natural gas is required to compensate the reduction of heat extracted from the ambient air as its temperature decreases. For a given ambient temperature, the mass flow rate of the required natural gas firstly decreases and then increases as the condensation temperature the ORC system increases from 55 to 62 °C, leading to a minimum value when the ORC condensation temperature is around 61 °C.

Fig. 4 presents the variation of mass flow rate of fresh air as ambient temperature varies. It is determined by the heat required in the Evaporator-HP and the residual heat carried by the flue gases. We can control the mass flow rate of the natural gas burnt in the burner to control the temperature of the mixture of fresh air and flue gases before they enter the Evaporator-HP. For the combined ORC-HP system, the thermal energy leaving it has two parts: the heat output carried away by the hot water, which is kept constant as 20 kW; and the thermal energy carried away by the gas mixture exiting the Evaporator-HP. The energy input also includes two parts: the heat produced by the combustion of natural gas and the heat extracted from fresh air flowing in the system. According to the first law of thermodynamic, all the energy entering the system should equate to the energy leaving it. Hence, the variation trend of mass flow rate of fresh air in Fig. 4 is opposite to that of the mass flow rate of natural gas as shown in Fig. 3.

In general, for a given condensation temperature within the Condenser-ORC, as

562 the ambient air temperature increases, the mass flow rate of air increases so more heat
563 can be extracted from it (see Fig. 4), and less natural gas is needed (see Fig. 3). For a
564 given ambient temperature, as the condensation temperature of ORC increases from
565 55 to 62 °C, the required air flow rate firstly increases and then decreases.

566 Figures 5 and 6 present the effects of the ambient air temperature and the ORC
567 condensation temperature on the heat capacities of heat exchangers, including the
568 Condenser-HP, Condenser-ORC, and the post heater. In Fig. 5, heat capacities of both
569 the Condenser-HP and the post heater increase as the ambient air temperature
570 increases, while that of the Condenser-ORC decreases, when the total heat output is
571 kept as 20 kW. As the temperature of ambient air increases, the evaporating
572 temperature of the heat pump and the exiting temperature T_{15} rises. On the one hand,
573 more heat energy can be extracted from the mixture of fresh air and flue gases via the
574 Evaporator-HP. Consequently, the water temperature T_{12} increases. On the other hand,
575 less natural gas is needed in the burner, and consequently less power output is
576 generated by the ORC system for a given condensation temperature in the
577 Condenser-ORC. As a result, the heat capacity of Condenser-ORC decreases.

578 In Fig. 6, the ambient temperature is kept constant at 5 °C. The heat capacity of
579 the post heater firstly decreases as the ORC condensation temperature increases, and
580 then stays constant when it is above 60 °C. This is due to a fixed temperature T_6. The
581 calculated heat capacities of the two condensers both increase as the ORC
582 condensation temperature increases. This can be attributed to that the temperature of
583 flue gases is set as above 120 °C to prevent corrosion in the Evaporator-ORC.

584 Figure 7 presents the share of the heat supply to the water through those three
585 heat exchangers under various operational conditions. Interestingly, the results clearly
586 show that the heat supply is dominated by the two condensers (i.e., Condenser-HP and
587 Condenser-ORC), while the heat supplied through the post heater is marginal. For a
588 given ORC condensation temperature, the variation of ambient air temperature has
589 little effect on the distribution of heat supply. It can also be seen that, for a given
590 ambient air temperature, the ORC condensation temperature can strongly affect the
591 distribution of heat supply. For example, when T_0=5 °C, the heat supplied by the post
592 heater decreases from 13.61% to 1.42% when the ORC temperature increases from 55
593 to 61 °C. From the analysis above, it can be inferred that the post heater can only
594 supply very limited amount of heat to the water, especially when ORC condensation
595 temperature is high. Hence, it might be beneficial to remove it from the system to
596 improve the overall cost-effectiveness.

597 Figures 8, 9 and 10 show the calculated heat transfer area of the Condenser-HP,
598 Condenser-ORC, and the post heater, respectively. According to Equation (39), the
599 heat transfer area of each heat exchanger depends on the heat capacity, the heat
600 transfer coefficient and LMTD.

601 In Fig. 8, for a given ORC condensation temperature, the heat transfer area of
602 Condenser-HP decreases as the ambient temperature increases. As mentioned in the
603 modelling section, the heat transfer area of the Condenser-HP is divided into two parts,
604 the single phase part from State 8 to State E (see in Fig. 2) and the condensation
605 process (two phase) part from State E to State 9. The variation of ambient temperature

directly affects the condensation temperature of the heat pump. As the ambient temperature increases, the heat transfer coefficient of both single phase and condensation process increase due to a higher condensation temperature in the heat pump. The LMTD of condensation process part decreases while that of the single phase part increases. The combined effects of these factors will lead to a decrease in the heat transfer area of single phase part and an increase in condensation process part. As the reduction of heat transfer area in the single phase part is larger, the total heat transfer area of Condenser-HP presents a downward trend.

Figure 9 shows that, for a given ORC condensation temperature, the heat transfer area of Condenser-ORC decreases as the ambient temperature increases. Moreover, there exists a minimum heat transfer area of the Condenser-ORC, which first decreases and then increases when the ORC condensation temperature increases. The method used for the heat transfer area calculation of the Condenser-HP is also applied to calculate the heat transfer area of Condenser-ORC. As mentioned above, a higher ambient temperature will lead to a higher condensation temperature of the heat pump, thus a higher water temperature T_{12} and a higher heat transfer coefficient. The LMTD of single-phase part decreases, while that of the condensation process part increases. Similarly, the heat transfer area of Condenser-ORC increases with the ambient temperature.

In the post heater, the heat transfer area is calculated by using the correlation for the single-phase since no phase change happens during the heat transfer process. It is clearly shown in Fig. 10 that the heat transfer area of the post heater decreases with

628 the increasing ambient temperature and condensation temperature. As the ambient
629 temperature increases, the inlet temperatures of flue gases T_6 increases while the
630 water temperature T_{13} decreases. Although the heat capacity of the post heater
631 increases (see in Fig.5), the heat transfer area of the post heater decreases as both the
632 LMTD and heat transfer coefficient increase. Moreover, as the heat transfer
633 coefficient without phase change is much smaller than that with phase change, the
634 heat transfer area of the post heater with smaller heat capacity is even higher than that
635 of the two condensers.

636 A fin-and-tube heat exchanger is adopted for the Evaporator-HP because the heat
637 transfer area at the air side is much larger than other heat exchangers. In Fig. 11, the
638 left graph shows the calculated heat transfer area at fin side as a function of ORC
639 condensation temperature and ambient air temperature. In general, it increases as the
640 ambient air temperature increases for all tested ORC condensation temperatures. For a
641 given ambient temperature, the fin area firstly increases and then decreases as the
642 ORC condensation temperature increases from 55 to 62 °C. The right graph in Fig. 11
643 shows the calculated heat transfer areas at tube side as a function of ORC
644 condensation temperature and ambient air temperature. The variation of the required
645 heat transfer area of tube side is the similar to that of fin side since the ratio between
646 them remains constant.

647 The effect of the ORC condensation temperature on the thermal efficiency of
648 ORC is shown in Fig. 12. The results show that the thermal efficiency of the ORC
649 system decreases as its condensation increases. Ideally, a low condensation

temperature is preferred to obtain high thermal efficiency. However, trade-off is needed to achieve the maximum overall fuel-to-heat efficiency in the proposed system.

The *COP* of a heat pump strongly depends on the temperature lift between its evaporator and condenser. The exiting temperature T_{15} of the mixture should be lower than the ambient air temperature in order to extract heat energy from fresh air. Therefore, the evaporation temperature in the Evaporator-HP needs to be set below the ambient air temperature. Fig. 13 shows the calculated *COP* as a function of ambient air temperature for different ORC condensation temperatures. The results show that heat pump can reach a *COP* up to 5.56.

A fuel-to-heat efficiency is introduced in this research to evaluate the performance of different heating technologies. Fig. 14 shows that the calculated fuel-to-heat efficiency as a function of ambient air temperature and the ORC condensation temperature. In general, it increases as the ambient air temperature increases this is because the HP has a higher *COP* at higher ambient air temperature as shown in Fig. 13. For a given ambient temperature, it firstly increases and then decreases when the ORC condensation temperature increases. It reaches its maximum value at the condensation temperature of 61 °C. Among all the operation conditions considered, the fuel-to-heat efficiency reaches its maximum value of 1.47 when the ORC condensation temperature and the ambient temperature is 61 °C and 5 °C, respectively.

672 **4.3 Optimised model**

673 **4.3.1 Optimised working condition**

674 Through the analysis above, the integrated system can then be optimised to
675 achieve the maximum fuel-to-heat energy efficiency. One case with an ambient air
676 temperature of 5 °C is used as example to demonstrate an optimised model. The
677 optimum ORC condensation temperature was calculated as 61 °C as shown in Fig. 14.
678 The properties and key parameters of the optimised model are summarised in Tables 7
679 and 8.

680 Table 7 lists the properties of different state points of the combined cycles as
681 shown in Fig. 1. Table 8 shows the heat supply of the three heat exchangers. The
682 water is heated in Condenser-HP, Condenser-ORC, and post heater in series, and the
683 heat supply by these three heat exchangers are 9.42 kW, 10.29 kW, and 0.28 kW,
684 respectively. The natural gas flow rate is 0.000244 kg/s, and heat produced in the
685 burner is 13.66 kW. The Evaporator-ORC transfers 11.79 kW heat to the ORC system,
686 and it produces 1.81 kW shaft power. The HP extract 7.61 kW heat from the gas
687 mixture via the evaporator, and delivers 9.42 kW heat to the water via its condenser at
688 a temperature of 36.3 °C. The original purpose of using the post heater is to recover
689 heat from the flue gas. It is clearly shown that the heat supply by the post heater
690 accounts for only 1.41% of the total heat energy.

691

692 **4.3.2 Effect of post heater**

693 From the above analysis we can learn that the post heater plays limited role,

694 especially for a relative high ORC condensation temperature. Therefore, the system
695 performance of the model without post heater was investigated in this part and the
696 results are compared with that of the model with post heater.

697 As shown in Table 9, for both models, the thermal efficiency of the ORC
698 subsystem and the COP of the heat pump subsystem are more or less the same, while
699 the fuel-to-heat efficiency of system without a post heater is a bit smaller than that of
700 the system with a post heater. After removing the post heater, the temperature of
701 exhaust gas T_{17} becomes higher, which will require less fresh air since the evaporation
702 temperature in Evaporator-HP is fixed. As a result, less energy can be exacted from
703 the ambient air thus lead to a slightly lower fuel-to-heat efficiency.

704

705 **5. Conclusion**

706 This paper proposes a novel natural gas fuelled water heater that essentially
707 integrates an ORC power plant with a heat pump, with waste heat recovery. Heat
708 energy produced from combustion of natural gas in a burner powers an ORC power
709 plant. The generated power directly drives a vapour compression cycle heat pump.
710 Cold tap water is heated by several heat exchangers in series to gradually increase its
711 temperature. The flue gas exiting is mixed with ambient air to further extract its
712 residual heat in the evaporator of the heat pump.

713 The simulation results demonstrated that the proposed system has great potential
714 to improve the efficiency of domestic hot water applications. The advantages of the
715 proposed system include:

716 (1) Unlike using a heat pump to directly heat cold tap water to the required
717 temperature, the proposed system raises the water temperature using several heat
718 exchangers in series, so the condensation temperature of the heat pump can be
719 significantly reduced, leading to a much higher *COP*.

720 (2) The waste heat of the ORC power cycle and flues have been recovered, so the
721 overall fuel-to-heat energy utilisation efficiency of natural gas can be maximised.

722 (3) The proposed system can adjust the heating loads between the
723 Condenser-ORC and Condenser-HP when the ambient air temperature varies.

724 (4) The mechanical power of expander of the ORC cycle directly drives the
725 compressor of the heat pump, so it eliminates the electrical generator or motor, and
726 thus avoids the transduction losses

727 (5) For all the tested conditions, the research results show that there is an
728 optimum ORC condensation temperature of 61 °C to deliver hot water at 65 °C when
729 the ambient air temperature is 5 °C, leading to a maximum fuel-to-heat efficiency of
730 147%.

731 (6) It was also found that the post heater could only provide a very small amount
732 of heat supply. From the thermodynamic point of view, a post heater could slightly
733 improve the fuel-to-heat efficiency. However, from viewpoint of cost-effectiveness, it
734 may be removed from the proposed system so the whole system and control strategy
735 can be largely simplified.

736 In a summary, this research shows that the proposed natural gas fuelled water
737 heater can potentially achieve a much higher fuel-to-heat energy efficiency than other

738 gas fuelled heating technologies. It has great potential to make a contribution to the
739 carbon reduction of domestic heating sector.
740
741 **Acknowledgment**
742 This research is funded by EPSRC (EP/N020472/1, EP/N005228/1,
743 EP/R003122/1, and EP/P028829/1) in the United Kingdom.
744
745 **Reference**
746 [1] Department for Energy and Climate Change (DECC), United Kingdom Housing
747 Energy Fact File 2012 [online], Publication URN: 12D/354, Available at
748 URL: https://www.gov.uk/government/uploads/system/uploads/attachmentdata/file/20
749 1167/ukhousingactfile2012.pdf/>, 2012
750 [2] DECC. The future of heating: a strategic framework for low carbon heating in the
751 UK, 2012.
752 [3] Self SJ, Reddy BV, Rosen MA. Geothermal heat pump systems: Status review and
753 comparison with other heating options [J]. Applied Energy, 2013, 101: 341-8.
754 [4] Wu W, Wang B, Shi W, et al. Absorption heating technologies: a review and
755 perspective [J]. Applied Energy, 2014, 130:51-71.
756 [5] The Energy Saving Trust: Getting Warmer: A Field Triel of Heat Pumps, 2010.
757 [6] UK Government: The UK Low Carbon Transition Plan.
758 [7] Critoph RE: Gas-Driven Heat Pumps: Market Potential, Support Measures and
759 Barriers to development in the UK Market., DECC, 2013.

760 [8] Fischer D, et al., Comparison of control approaches for variable speed air source
761 heat pumps considering time variable electricity prices and PV [J]. Applied Energy,
762 2017, 204: 93-105.
763 [9] Hu B, Li Y, Cao F, et al, Extremum seeking control of COP optimization for
764 air-source transcritical CO_2 heat pump water heater system [J]. Applied Energy, 2015,
765 1;147:361-72.
766 [10] Gupta R, Irving R, Development and application of a domestic heat pump model
767 for estimating CO_2 emissions reductions from domestic space heating, hot water and
768 potential cooling demand in the future [J]. Energy and Buildings, 2013, 60: 60-74.
769 [11] Hewitt NJ, Huang MJ, Anderson M, et al. Advanced air source heat pumps for
770 UK and European domestic buildings [J]. Applied Thermal Engineering, 2011,
771 31(17):3713-19.
772 [12] Eyre N, Baruah P. Residential heating policy for a low carbon world: A case
773 study of UK scenarios[C]//Proc. ACEEE Summer Study Energy Eff. Bldgs, 2014.
774 [13] Love J, Smith AZ, Watson S, et al. The addition of heat pump electricity load
775 profiles to GB electricity demand: Evidence from a heat pump field trial [J]. Applied
776 Energy, 2017, 204:332-42.
777 [14] Strong DTG, Development of a directly fired domestic heat pump, Ph.D. Thesis,
778 University of Oxford, UK 1980.
779 [15] Demierre J, Henchoz S, Favrat D. Prototype of a thermally driven heat pump
780 based on integrated Organic Rankine Cycles (ORC) [J]. Energy, 2012, 41(1)10-17.
781 [16] Demierre J, Favrat D, Schiffmann, et al. Experimental investigation of a

782 Thermally Driven Heat Pump based on a double Organic Rankine Cycle and an
783 oil-free Compressor-Turbine Unit [J]. International Journal of Refrigeration, 2014, 44:
784 91-100.
785 [17] Wan X, Cai L, Yan J, et al., Power management strategy for a parallel
786 hybrid-power gas engine heat pump system [J]. Applied Thermal Engineering,
787 2017, 110: 234-43.
788 [18] Shang S, Li X, Wu W, et al., Energy-saving analysis of a hybrid power-driven
789 heat pump system [J]. Applied Thermal Engineering, 2017, 123:1050-9.
790 [19] Cho H, Sarwar R, Mago P, et al. Design and Feasibility Study of Combined Heat
791 and Power Systems Integrated with Heat Pump [J]. Applied Thermal Engineering,
792 2016, 93: 155-65.
793 [20] Kang S, Li H, Lei J, et al. A new utilisation approach of the waste heat with
794 mid-low temperature in the combined heating and power system integrating heat
795 pump [J]. Applied Energy, 2015, 160:185-93.
796 [21] Schimpf S, Span R. Simulation of a Solar Assisted Combined Heat
797 Pump-Organic Rankine Cycle System [J]. Energy Conversion and Management, 2015,
798 102:151-60.
799 [22] Liu H, Zhou Q, Zhao H, et al. Experiments and Thermal Modelling on Hybrid
800 Energy Supply System of Gas Engine Heat Pumps and Organic Rankine Cycle [J].
801 Energy and Buildings, 2015, 87: 226-32.
802 [23] Siviter J, Montecucco A, Knox AR. Rankine cycle efficiency gain using
803 thermoelectric heat pumps [J]. Applied Energy, 2015, 140:161-70.

804 [24] Siddiqi MA, Atakan B. Alkanes as fluids in Rankine cycles in comparison to
805 water, benzene and toluene [J]. Energy, 2012, 30;45(1):256-63.
806 [25] Shu G, Li X, Tian H, et al. Alkanes as working fluids for high-temperature
807 exhaust heat recovery of diesel engine using organic Rankine cycle [J]. Applied
808 Energy, 2014, 15;119:204-17.
809 [26] Zhu Y, Jiang L, Jin V, et al. Impact of built-in and actual expansion ratio
810 difference of expander on ORC system performance [J]. Applied Thermal
811 Engineering, 2014, 5;71(1):548-58.
812 [27] Castro JB, Urchueguía JF, Corberán JM, et al. Optimized design of a heat
813 exchanger for an air-to-water reversible heat pump working with propane (R290) as
814 refrigerant: Modelling analysis and experimental observations [J]. Applied thermal
815 engineering, 2005, 25(14):2450-62.
816 [28] Liu N, Xiao H, Li J. Experimental investigation of condensation heat transfer and
817 pressure drop of propane, R1234ze (E) and R22 in minichannels [J]. Applied Thermal
818 Engineering, 2016, 102:63-72.
819 [29] Pitarch M, Navarro-Peris E, Gonzálvez-Maciá J, et al. Experimental study of a
820 subcritical heat pump booster for sanitary hot water production using a subcooler in
821 order to enhance the efficiency of the system with a natural refrigerant (R290) [J].
822 International Journal of Refrigeration, 2017, 73:226-34.
823 [30] Hung TC. Waste heat recovery of organic Rankine cycle using dry fluids [J].
824 Energy Conversion and management, 2001, 42(5): 539-53.
825 [31] Shu G, Liu L, Tian H, et al. Parametric and working fluid analysis of a dual-loop

826 organic Rankine cycle (DORC) used in engine waste heat recovery [J]. Applied
827 energy, 2014, 113:1188-98.
828 [32] Qu M, Abdelaziz O, Yin H. New configurations of a heat recovery absorption
829 heat pump integrated with a natural gas boiler for boiler efficiency improvement
830 [J]. Energy Conversion and Management, 2014, 87:175-84.
831 [33] Terhan M, Comakli K. Energy and exergy analyses of natural gas-fired boilers in
832 a district heating system [J]. Applied Thermal Engineering, 2017, 121:380-87.
833 [34] Che D, Liu Y, Gao C. Evaluation of retrofitting a conventional natural gas fired
834 boiler into a condensing boiler [J]. Energy Conversion and Management, 2004,
835 45(20):3251-66.
836 [35] Bowman CT. Control of combustion-generated nitrogen oxide emissions:
837 technology driven by regulation [J]. In Symposium (International) on Combustion,
838 1992, 24(1): 859-78.
839 [36] Turns SR. An introduction to combustion (Vol. 287). New York: McGraw-hill,
840 1996.
841 [37] Dai X, Shi L, An Q, Qian W. Screening of hydrocarbons as supercritical ORCs
842 working fluids by thermal stability [J]. Energy Conversion and Management.
843 2016,126:632-7.
844 [38] Vaja I, Gambarotta A. Internal combustion engine (ICE) bottoming with org,nic
845 Rankine cycles (ORCs) [J]. Energy, 2010, 35(2): 1084-93.
846 [39] Kakaç S (Sadık), Liu H. Heat exchangers: selection, rating, and thermal design
847 [J]. Tribology & Lubrication Technology, 2012.

[40] Shu G, Yu G, Tian H, et al. A multi-approach evaluation system (MA-ES) of Organic Rankine Cycles (ORC) used in waste heat utilization [J]. Applied Energy, 2014, 132: 325-38.

[41] Kandlikar SG. A general correlation for saturated two-phase flow boiling heat transfer inside horizontal and vertical tubes [J]. ASME J. Heat Transfer, 1990, 112(1): 219-28.

[42] Kandlikar SG. An Improved Correlation for Predicting Two-Phase Flow Boiling Heat Transfer Coefficient in Horizontal and Vertical Tubes [J]. HTD (Publ.) (Am. Soc. Mech. Eng.); (United States), 1983, htd-vol-27.

[43] Drescher U, Brüggemann D. Fluid selection for the Organic Rankine Cycle (ORC) in biomass power and heat plants [J]. Applied thermal engineering, 2007, 27(1):223-8.

861

Nomenclature

B_o	Boiling number	S	Entropy
b_1	Corrugation depth	S_1	Depth of the heat exchanger perpendicular to airflow direction
C_o	Convection number	S_2	Depth of the heat exchanger in airflow direction
c_p	Specific heat at constant pressure	S_f	Fin spacing
COP	Coefficient of performance	t	Plate thickness
d_0	Tube outside diameter	T	temperature
d_{am}	Mean humidity ratio of wet air	υ	Kinematic viscosity
d_{eq}	Equivalent diameter	W	Mechanical work
di	Internal diameter of tube	W_f	Face velocity
F_{fl}	Fluid-dependent parameter	x	Quality
Frl	Froude number with all flow as liquid	δ_f	Fin thickness
g	Acceleration due to gravity	ρ	Density
G	mass flux of the working fluid	μ	Dynamic viscosity
h	Enthalpy	β	Chevron angle
ΔH	Combustion heat	λ	thermal conductivity
i_{fg}	Enthalpy of vaporization	δ_f	Thickness of the fin
k_1	Correction coefficient of configuration	α	Heat transfer coefficient
k_2	Correction coefficient of fin style	ϕ	Surface enlargement factor
Lw	Plate width	α	heat transfer coefficient
m	Mass flow rate	η	efficiency
M	Molar mass		
Nu	Nusselt number	Acronyms	
P_{cr}	Critical pressure	ORC	organic Rankine cycle
Pr	Prandtl number	HP	Heat pump
Q	heat capacity	CHP	Combined heat and power
r_0	Fouling resistance of tube side	COP	Coefficient of performance
r_1	Fouling resistance of fin side	PPTD	Pinch point temperature difference
Re	Renold number	LMTD	Logarithmic mean temperature difference
Rp	Mean asperity height		

862

863

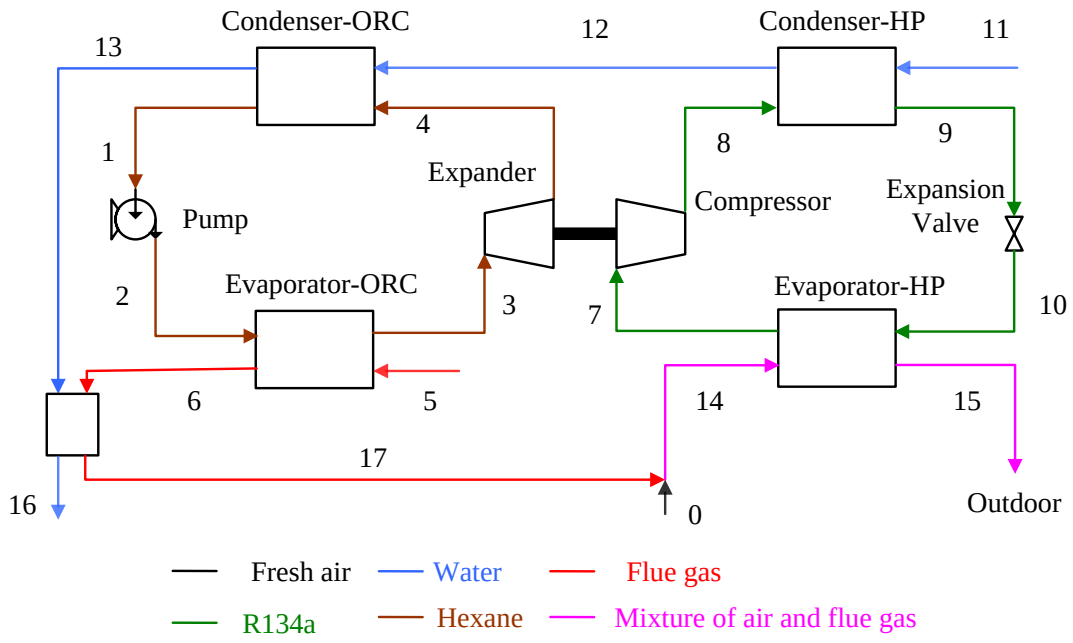

Fig.1 Schematic diagram of the proposed natural gas fuelled water heater system

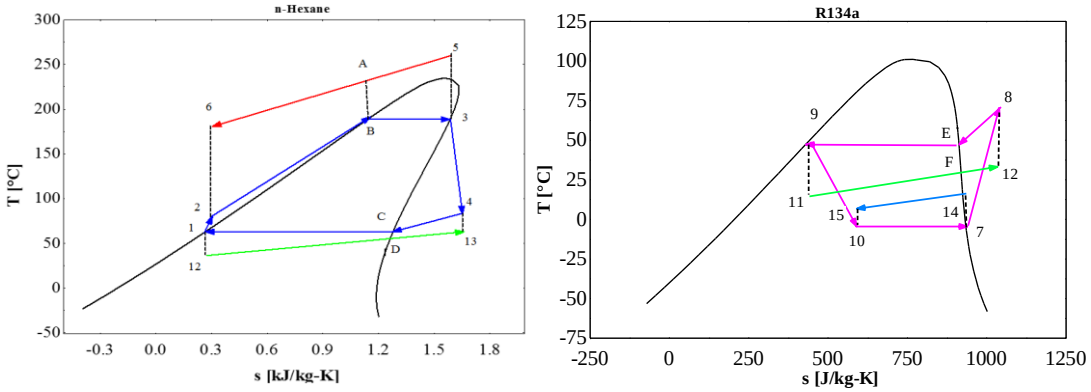

Fig.2 Temperature-Entropy diagrams of both the ORC (hexane) and heat pump cycle (R134a)

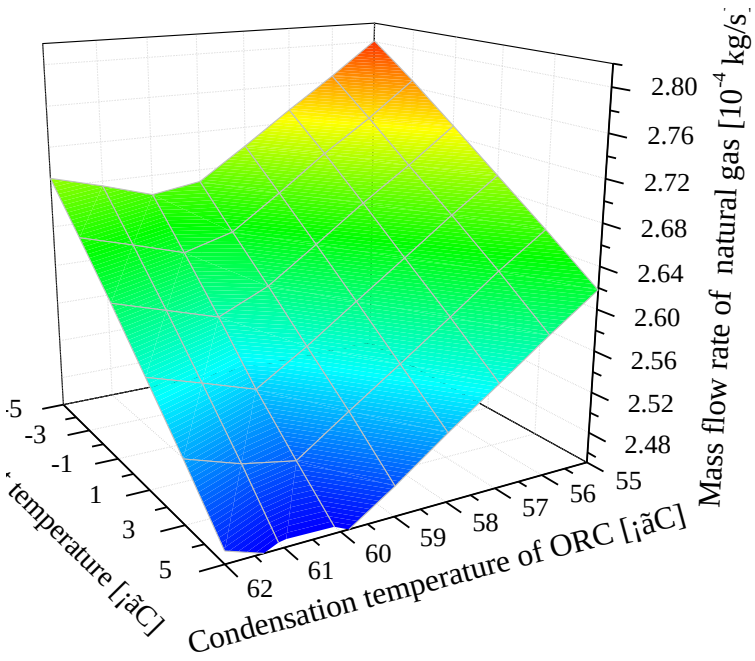

Fig.3 The required natural gas for delivering 20 kW at 65 °C hot water supply to match different ambient temperatures and ORC condensation temperatures

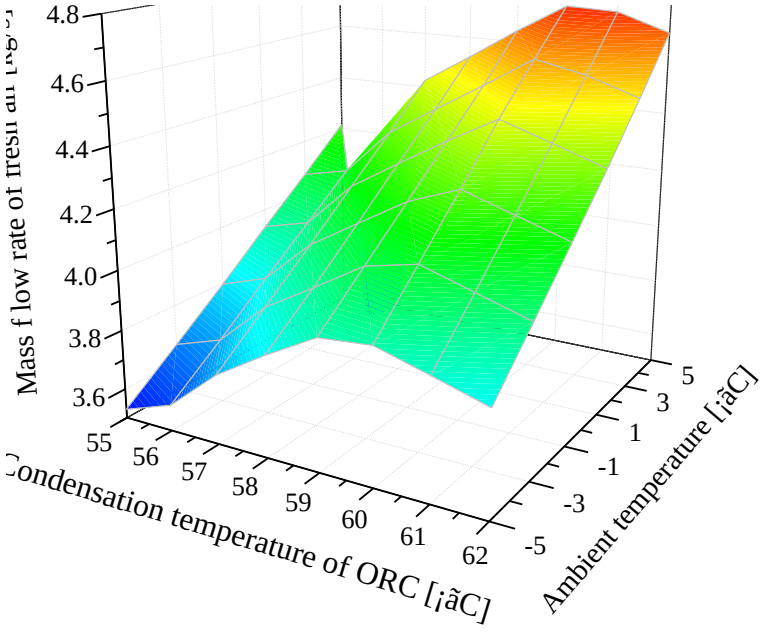

Fig.4 The required fresh air to be mixed with the flue gas before entering the inlet of Evaporator-HP to match the different ambient temperature

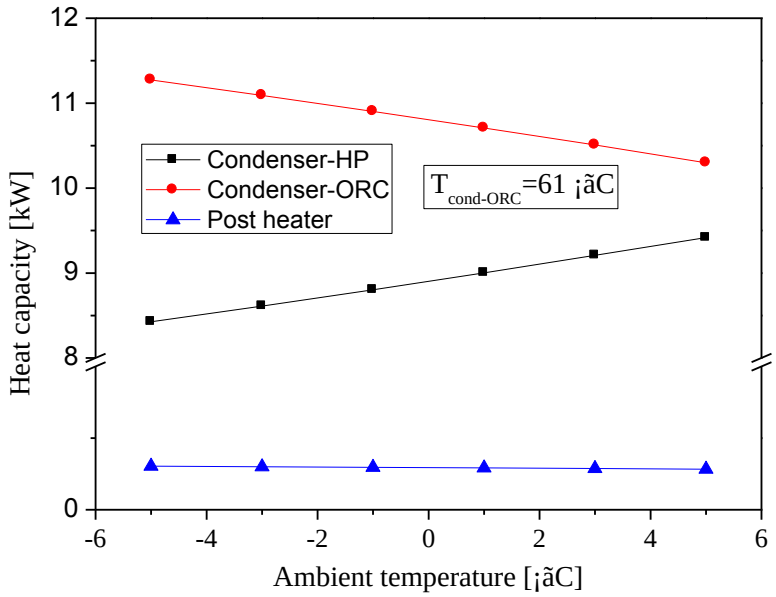

Fig.5 Heat capacities of the three heat exchangers of the system for a given ORC condensation temperature of 61 °C

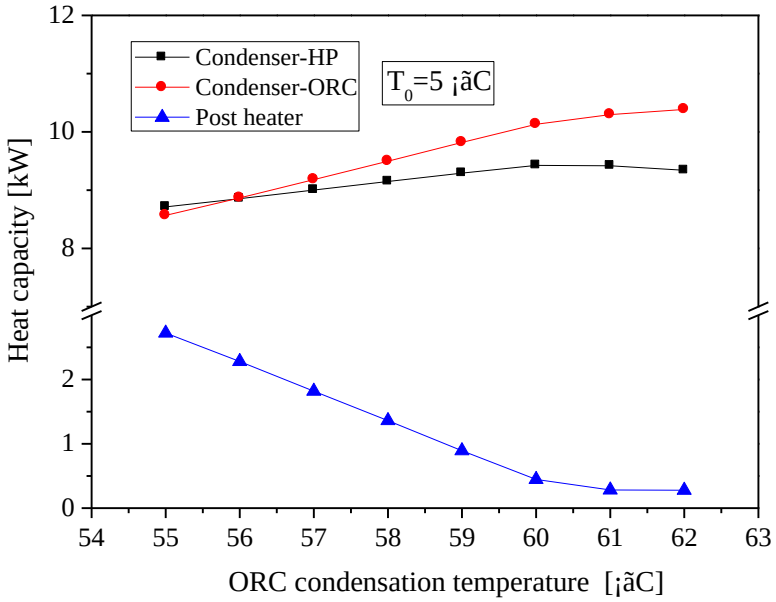

Fig.6 Heat capacities of the three heat exchangers of the system for a given ambient air temperature of 5 °C

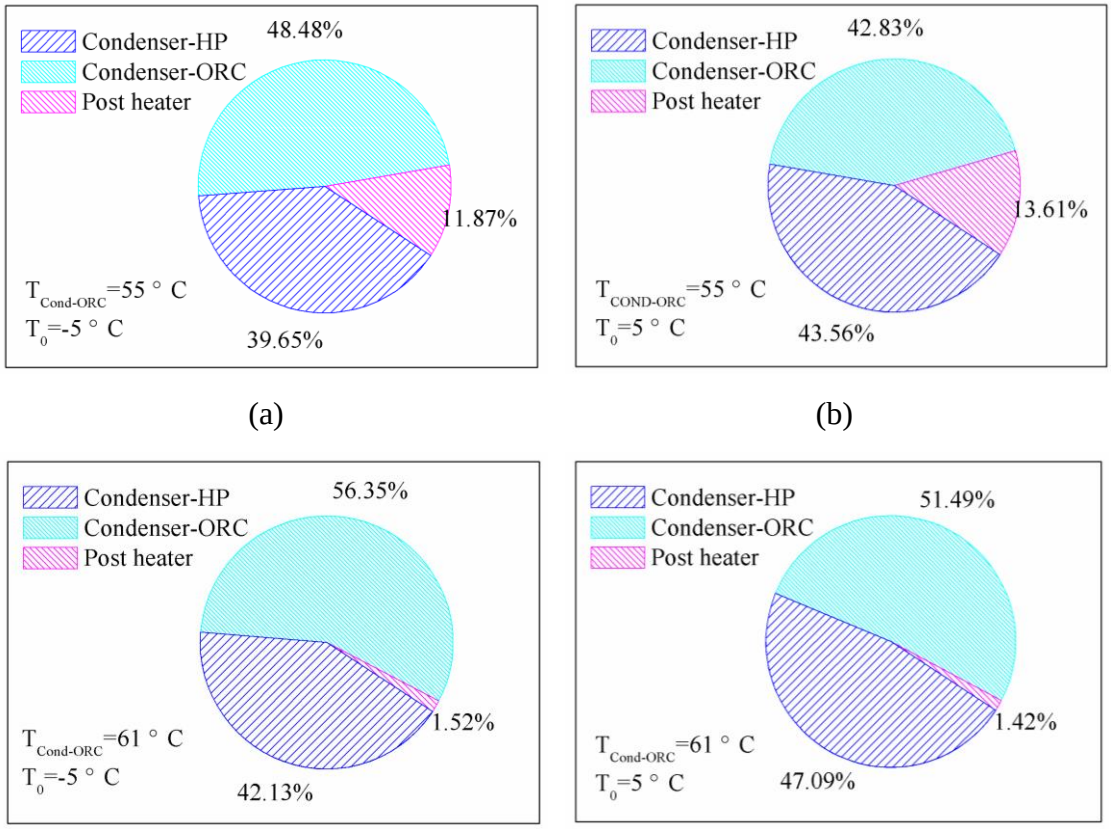

Fig.7 Share of heat supply by the three heat exchangers under different optional conditions: (a) $T_{cond\text{-}ORC}$=55 °C and T_0=-5 °C; (b) $T_{cond\text{-}ORC}$=55 °C and T_0=5 °C; (c) $T_{cond\text{-}ORC}$=61 °C and T_0=-5 °C; (d) $T_{cond\text{-}ORC}$=61 °C and T_0=5 °C;

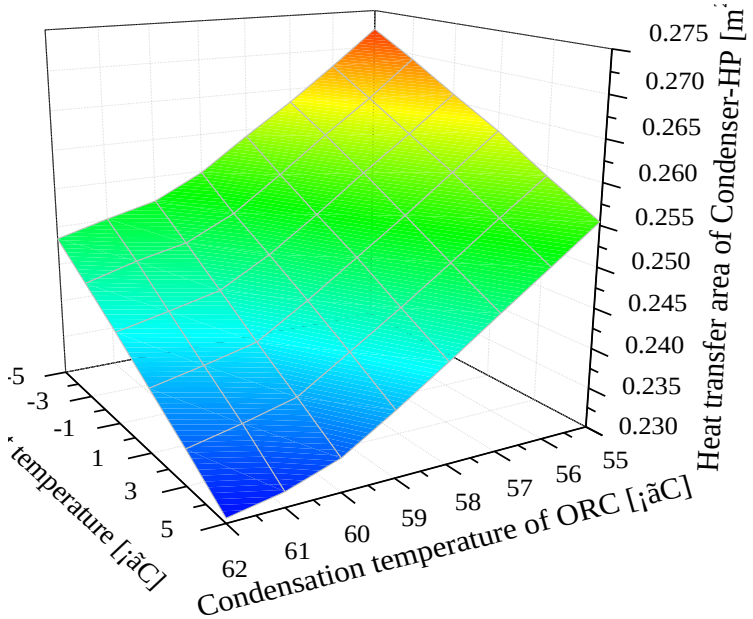

Fig.8 The required heat transfer area of the Condenser-HP

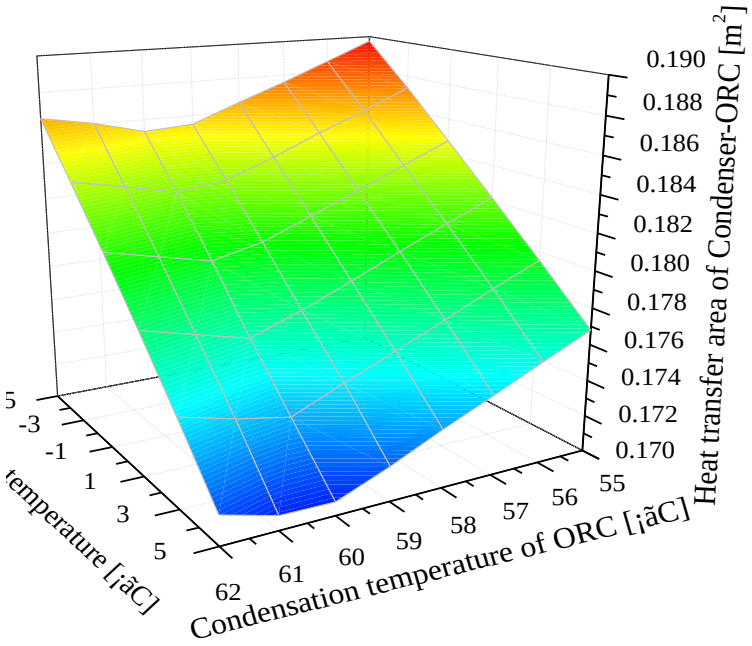

Fig.9 The required heat transfer area of the Condenser-ORC

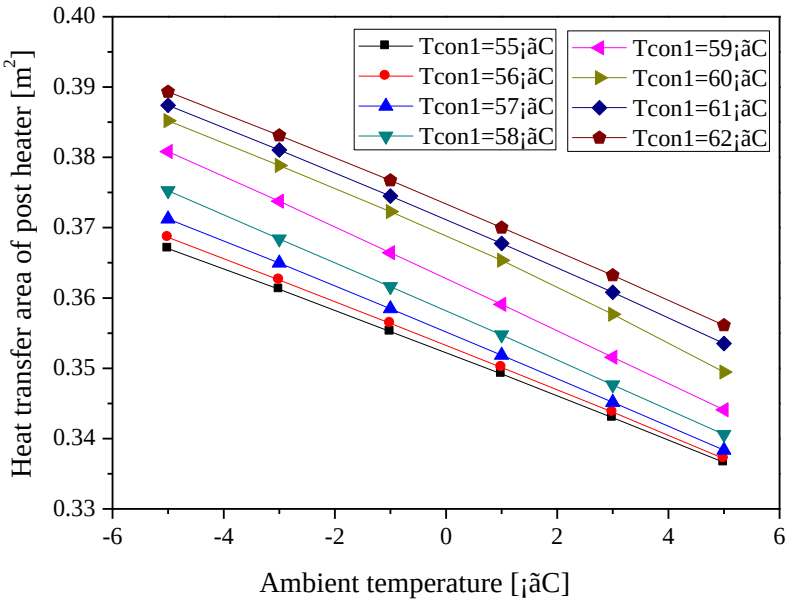

Fig.10 The required heat transfer area of Post heater

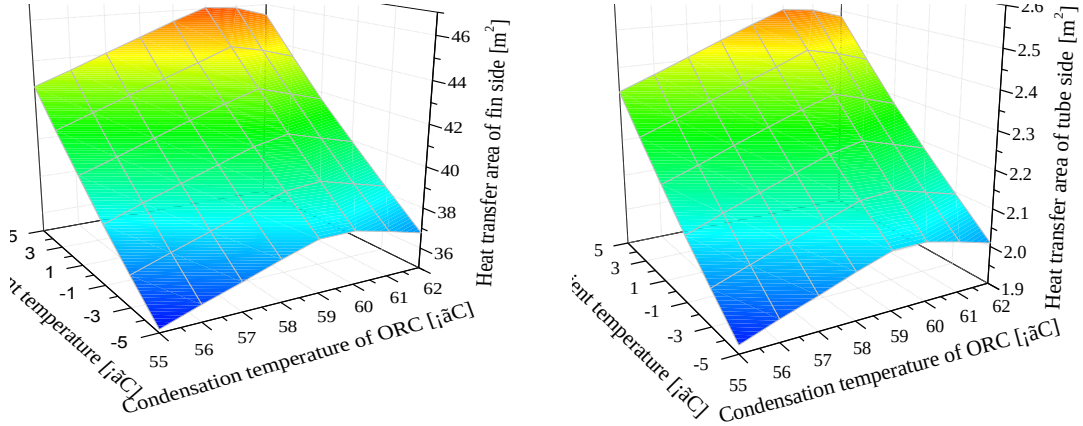

(a) fin side (b) tube side

Fig. 11 The required heat transfer area of both the fin side and tube side of the Evaporator-HP

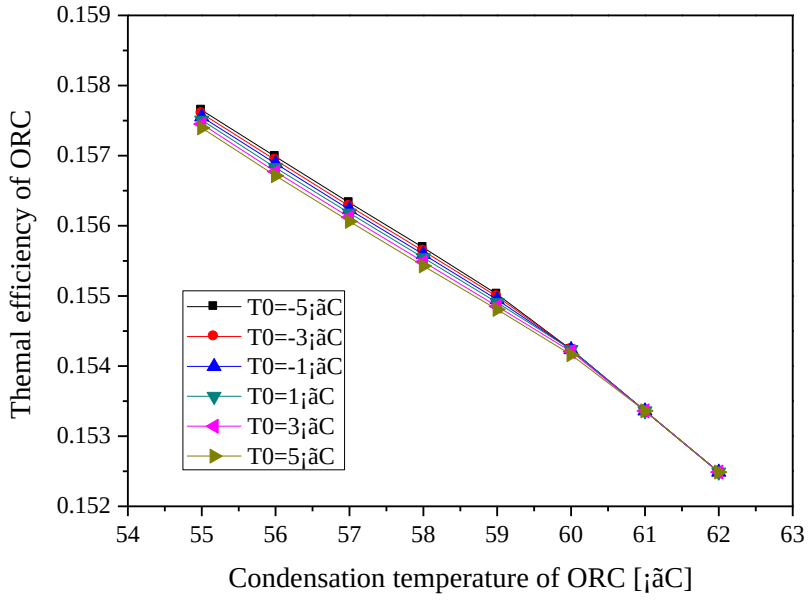

Fig. 12 The effect of ORC condensation temperature on thermal efficiency of ORC

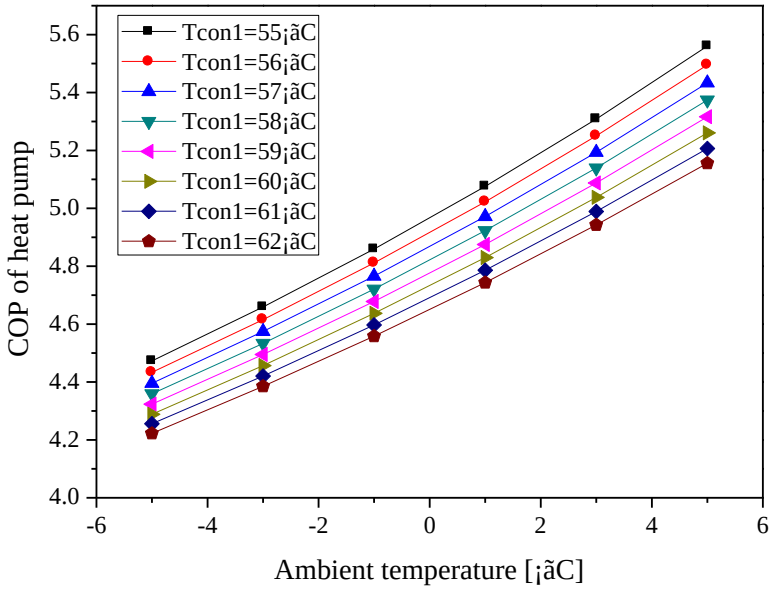

Fig.13 The effect of ambient temperature on the *COP* of the heat pump

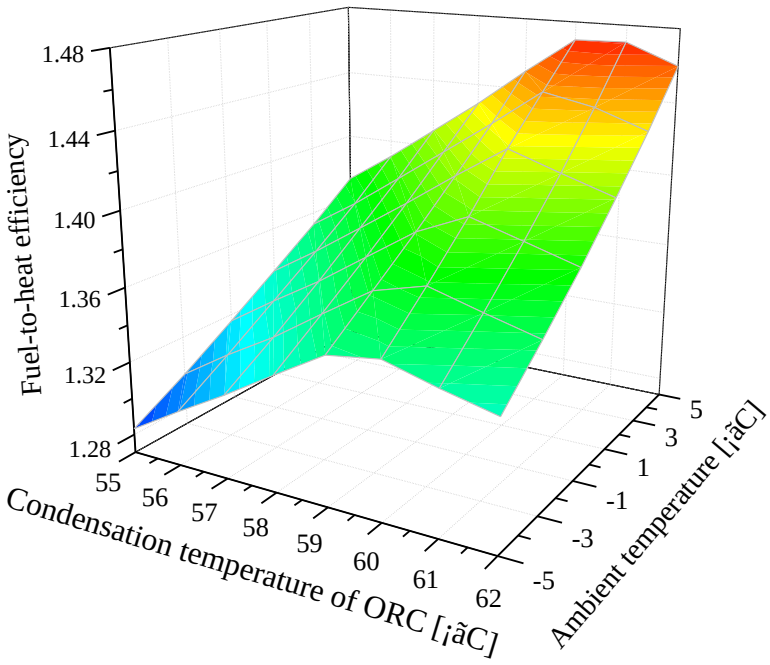

Fig.14 The fuel-to-heat efficiency against ambient temperature and ORC condensation temperature

935 Table 1 Key operating parameters of the combined cycles

Parameters	value
Atmosphere pressure, P_0 [kPa]	101
Efficiency of pump, η_1	0.9
Efficiency of turbine, η_2	0.7
Efficiency of compressor, η_3	0.7
Efficiency of combustion, η_4	1
Temperature of return water, T_{11} [°C]	10
PPTD in evaporator of ORC, [°C]	30
PPTD in Post heater, [°C]	5
PPTD in condenser of heat pump, [°C]	5

936
937
938
939 Table 2 Key geometric dimensions of plate heat exchangers [42]

Parameters	value
Chevron angle β [degree]	60
Surface enlargement factor, ϕ [/]	1.117
Plate width, *Lw*[m]	0.119
Plate thickness, *t* [m]	0.0003
Mean asperity height, *Rp*[μm]	0.3
Corrugation depth, b_1 [m]	0.00224
Equivalent diameter of liquid side, *deq* [m]	0.004
Equivalent diameter of gas side,*deqg* [m]	0.009
Coefficient of thermal conductivity, λ [kW/(m·K)]	0.00163

940
941

Table 3 Key geometric dimensions of fin and tube heat exchangers

Parameters	value
Tube outside diameter,d_0[m]	0.00952
Depth of the heat exchanger perpendicular to airflow direction,S_1[m]	0.0254
Depth of the heat exchanger in airflow direction,S_2[m]	0.022
Fin spacing, S_f[m]	0.0002
Thickness of the fin,δ_f[m]	0.000014
Face velocity, W_f[m/s]	3
Fouling resistance of tube side, r_0[m^2K/kW]	2.5
Fouling resistance of fin side, r_1 [m^2K/kW]	1
Thermal conductivity of copper, λ_c[kW/(m·K)]	0.383
Thermal conductivity of aluminium, λ_{al}[kW/(m·K)]	0.22
Mean humidity ratio of wet air, d_{am} [g/kg]	5.1

Table 4 Parameters of the combined cycle

Parameter	Heat pump cycle			Parameter	ORC cycle		
	ASPEN Plus	Refprop/ Matlab	Difference		ASPEN Plus	Refprop/ Matlab	Difference
T_{12}, K	307.05	306.48	0.2%	T_{13}, K	330.73	333.68	0.9%
T_{con2}, K	305.75	307.98	0.7%	T_{con1}, K	326.08	326.15	0
T_{eva2}, K	270.33	270.33	0	T_{eva1}, K	507.15	506.93	0
T_{15}, K	274.55	274.55	0	$Q_{con\text{-}ORC}$, kW	9.89	10.36	4.8%
$Q_{con\text{-}HP}$, kW	10.01	9.86	1.5%	$Q_{eva\text{-}ORC}$, kW	11.63	12.14	4.4%
$Q_{eva\text{-}HP}$, kW	8.18	7.94	2.9%	W_{ORC}, kW	1.84	1.92	4.3%
m_{f2}, kg/s	0.054	0.054	0	m_{f1}, kg/s	0.019	0.020	5.6%
W_{com}, kW	1.84	1.92	4.3%	W_p, kW	0.100	0.105	5.4%
Q_{post}, kW	1.16	1.13	2.8%	T_{17}, K	333.15	335.61	0.7%

Table 5 Evaluation of System performance

	ASPEN Plus	Refprop/Matlab	Difference
Combusted energy of fuel	15.6	15.6	0
COP of heat pump	5.45	5.14	5.7%
ORC thermal efficiency, %	14.92	14.96	0.3%
Overall fuel-to-heat efficiency	136.0	137.2	0.9%
Total heat absorbed by water, kW	21.07	21.36	1.4%

Table 6 Comparison of system performance using different ORC working fluids

	Fuel-to-heat efficiency			Thermal efficiency			*COP*		
Working fluid	hexane	R245fa	R123	hexane	R245fa	R123	hexane	R245fa	R123
T_0=-5	1.343	1.208	1.254				4.26	4.91	4.65
T_0=-3	1.366	1.224	1.271				4.42	5.12	4.85
T_0=-1	1.389	1.240	1.288	0.15	0.11	0.13	4.60	5.36	5.05
T_0=1	1.414	1.257	1.307				4.79	5.61	5.28
T_0=3	1.441	1.275	1.327				4.99	5.87	5.52
T_0=5	1.471	1.296	1.349				5.21	6.16	5.78

Table 7 Parameters of different states at optimal condition

state	T(°C)	P(kPa)	x
1	61	79	0
2	62.2	3000	0
3	233.8	3000	1
4	139.0	79	1
5	1809	101	1
6	120	101	1
7	0.5	298	1
8	51.7	958	1
9	37.8	958	0
10	0.5	298	0.26
11	10	101	0
12	36.3	101	0
13	65.1	101	1
14	5.1	101	1
15	3.5	101	1
16	65.9	101	1
17	71.7	101	1

Table 8 Heat transfer rate and power transfer of the key components

Parameters	Value
Heat capacity of Condenser-ORC, kW	10.29
Heat capacity of Condenser-HP, kW	9.42
Heat capacity of the Post Heater, kW	0.28
Mass flow rate of natural gas, kg/s	0.000244
Heat produced by the burner, kW	13.66
Heat capacity of Evaporator-ORC, kW	11.79
Power generated in Expander, kW	1.81
Mechanical work consumed by pump, kW	0.108
Mechanical work consumed by compressor, kW	1.81
Heat capacity of Evaporator-heat pump, kW	7.61
Thermal efficiency of ORC	15.34%
COP	5.21
Fuel-to-heat efficiency of the combined cycle	147.1%

964 Table 9 Comparison of system performance with and without post heater

	With post heater			Without post heater		
Ambient temperature	Fuel-to-heat efficiency	Thermal efficiency of ORC	*COP*	Fuel-to-heat efficiency	Thermal efficiency of ORC	*COP*
T_0=-5	1.343		4.256	1.323		4.256
T_0=-3	1.366		4.421	1.345		4.421
T_0=-1	1.389	0.153	4.597	1.369	0.153	4.597
T_0=1	1.414		4.786	1.394		4.786
T_0=3	1.441		4.989	1.421		4.989
T_0=5	1.471		5.206	1.450		5.206

965